ISSN (Print) 1226-1750
ISSN (Online) 2233-6656
Journal of Magnetics 30(4), 526-532 (2025) https://doi.org/10.4283/JMAG.2025.30.4.526

Directional Growth of Crystals and Orientation of Easy Magnetization Axis in Ce-Fe-Al-B Compounds

Meng-xue Liu[1,2], Peng-cheng Yang[1,2], Ji-zhong Zhao[1,2], Bang-chen Li[2], Suo Bai[2], and Zhu-bai Li[1,3]*

[1]*School of Science, Inner Mongolia University of Science and Technology, Baotou 014010, China*
[2]*School of Rare Earth Industry, Inner Mongolia University of Science and Technology, Baotou 014010, China*
[3]*Key Laboratory of Green Extraction & Efficient Utilization of Light Rare-Earth Resources, Ministry of Education, Baotou 014010, China*

(Received 15 July 2025, Received in final form 14 November 2025, Accepted 14 November 2025)

Ce element is abundant in rare-earth ore, and it is expected to substitute for Nd in $Nd_2Fe_{14}B$ to prepare permanent magnets. However, the crystal structure stability of $Ce_2Fe_{14}B$ is poor, and both $CeFe_2$ phase and α-Fe phase exist in $Ce_{14}(Fe,M)_{79.7}Al_{0.5}B_{5.8}$ strips prepared by rapid solidification. Via increasing the content of Al and reducing the content of B, α-Fe phase is eliminated in $Ce_{14}(Fe,M)_{78.9}Al_{1.6}B_{5.5}$ strips, and the columnar crystals are formed for the main phase of $Ce_2Fe_{14}B$ crystals. $CeFe_2$ phase is basically distributed in linear patterns, thinly coating on the surface of columnar crystals of $Ce_2Fe_{14}B$. Owing to Al atoms entering into $Ce_2Fe_{14}B$ crystals, the lattice entropy increases in $Ce_2Fe_{14}B$ crystals, and the melting point of the main phase increases. From the perspective of thermodynamics, it can enhance the stability of $Ce_2Fe_{14}B$ crystal structure. As the content of Al increases to 2.0 at.%, the columnar crystals are not formed in some areas due to the competitive growth of heterogeneous phases. These experiments indicate that by modifying the chemical composition in the Ce-Fe-Al-B compounds the crystal directional growth could be promoted, which should be beneficial to improve the orientation of easy magnetization axis in sintered magnets.

Keywords : Ce-Fe-Al-B compounds, columnar crystals, directional growth, crystal structure stability

1. Introduction

$Nd_2Fe_{14}B$ is rare-earth magnets, possessing high magnetocrystalline anisotropy, high coercivity and high remanence [1-3]. Rare-earth are the paragenesis ore, and Nd element is less abundant in rare-earth ore and much expensive. Ce is also the rare-earth element, which is much abundant and cheap, and so it is expected to prepare rare-earth magnets via Ce substituting for Nd [4-9]. It is noted that the ternary phase diagram of Ce-Fe-B is different from that of Nd-Fe-B [10, 11]. The stability of $Ce_2Fe_{14}B$ crystal structure is poor, and generally $Ce_2Fe_{14}B$ crystals can't grow directionally in the solidification process [12, 13]. The crystal structure stability is one of the keys for the preparation of rare-earth permanent magnets [14, 15]. Due to the high stability of crystal structure in Nd-Fe-B and the crystal anisotropy, the crystal growth is strongly directional dependence with the formation of columnar grains, and the columnar grains are separated by the thin intergranular phase [16, 17]. For the columnar grains it is easy to break into isolated particles along the intergranular phase through hydrogen decrepitation and jet mill [16], and the rotation of isolated particles under the applied pulsed field becomes easy for the orientation of the easy magnetization axis, and so the remanence is improved in the magnets [18]. Whereas in Ce-Fe-B alloys the directional growth of crystal grains is difficult and the minor phase of α-Fe may be formed in the solidification, resulting in the deterioration of magnetic properties. In order to enhance the crystal structure stability of Ce-Fe-B compounds for promoting the directional growth of crystals and the formation of columnar grains, the rare-earth elements of Nd and Gd would be added to form $RE_2Fe_{14}B$ crystal phase (RE is the abbreviation of rare-earth elements) [19, 20], and a small amount of elements such as Cu, Ga, Al, Zr and Ti would also be added to regulate the distribution of intergranular phases [21]. The elements of Cu, Ga, Zr and Ti are mainly distributed in the intergranular phases to improve the wettability of grain boundary and suppress

©The Korean Magnetics Society. All rights reserved.
*Corresponding author: Tel: +86-472-5953508
e-mail: lizhubai@imust.edu.cn

© 2025 Journal of Magnetics

the abnormal growth of grains [22, 23]. Different with the elements of Cu, Ga, Zr and Ti distributed mainly in the intergranular phases, Al atoms can enter the main phase [24], which may affect the structural stability of main phase. In this paper, the microstructure and the crystal structure stability were investigated in Ce-Fe-Al-B compounds by modifying the chemical composition, and it is expected to solve the difficulty in the directional growth of crystals in rare-earth Ce-Fe-based magnets.

2. Experimental

The strips were prepared, respectively, according to the atomic percentage formula of $Ce_{14}(Fe,M)_{79.7}Al_{0.5}B_{5.8}$, $Ce_{14}(Fe,M)_{79.4}Al_{1.1}B_{5.5}$, $Ce_{14}(Fe,M)_{78.9}Al_{1.6}B_{5.5}$ and $Ce_{14}(Fe,M)_{78.5}Al_{2.0}B_{5.5}$. Here M is the general term of the trace elements Cu, Ga, Zr and Ti, and their contents are 0.2 at.%, 0.1 at.%, 0.1 at.% and 0.1 at.%, respectively. The raw materials of Ce, Fe, Fe-B, Al, Cu, Ga, Zr and Ti were mixed according to the composition and putted into the crucible in a rapid solidification furnace. Under argon protection the mixture was inductively melted into the molten liquid, and then poured onto the rotating copper roll surface with the surface velocity of 1 m/sec to obtain the cast strips with the thickness of about 0.3 mm. The heat absorption of the strip was measured by NETZSCH STA449C Differential Scanning Calorimetry (DSC) with the temperature rising rate of 10 ℃/sec for phase transition temperature analysis. The phase composition was analyzed by BRUKER D8 Advance x-ray diffraction (XRD). The cross section of the strip was ground and polished, and the microstructure was detected by Model SUPRA55 Scanning electron microscope with backscattered electron (SEM&BSE), and the chemical component was measured by dot scanning with energy dispersive spectrometry (EDS).

The strips were ground into fine powder particles with a diameter of about 3.5 μm by hydrogen decrepition and nitrogen jet milling, and then pressed into green compacts after applying a pulsed magnetic field of 2T for powders alignment. The green compacts were sintered under the temperature of 960 ℃ to 1010 ℃ for 4 hours to obtain the densed magnets. The sintered magnet was ground into the powders for XRD measurements. The magnet was cut into thin sheet for the magnetization curve measurements by Quantum Design Versalab vibrating sample magnetometer (VSM) at temperature of 300 K. The microstructure was observed by SEM&BSE after polishing the surface of thin sheet, and the microtexture normal to the easy magnetization axis [001] was analyzed using electron backscatter diffraction (EBSD).

3. Results and Discussion

The microstructures of the cross section of the strip observed by SEM are shown in Fig. 1. The different brightness on the SEM maps is originated from the different scattering ability of atoms to electrons. The atoms mass of rare-earth Ce is highest and the electron scattering ability is strongest, so Ce-rich area and $CeFe_2$ phase are brighter. The gray areas are $Ce_2Fe_{14}B$ grains containing about 26 wt.% Ce, and as shown in Fig. 1(a), there are some dark parts masked in the box referring to α-Fe phase. The crystal structure stability of $Ce_2Fe_{14}B$ phase is weaker than that of $Nd_2Fe_{14}B$ phase [10,11], and more amount of impurity phases would be formed in the solidification process for Ce-Fe-B alloys. The melting point of α-Fe phase is higher than that of $Ce_2Fe_{14}B$ phase, and so it is easy to crystallize firstly for α-Fe phase. Reducing B content to 5.5 at.% and increasing Al content to 1.1 at.%, the phase of α-Fe is eliminated in the strips (shown in Fig. 1(b)). However, the distribution of $CeFe_2$ phase is still dispersed and discontinuous, and the main phase of $Ce_2Fe_{14}B$ crystals still has no a preferred growth

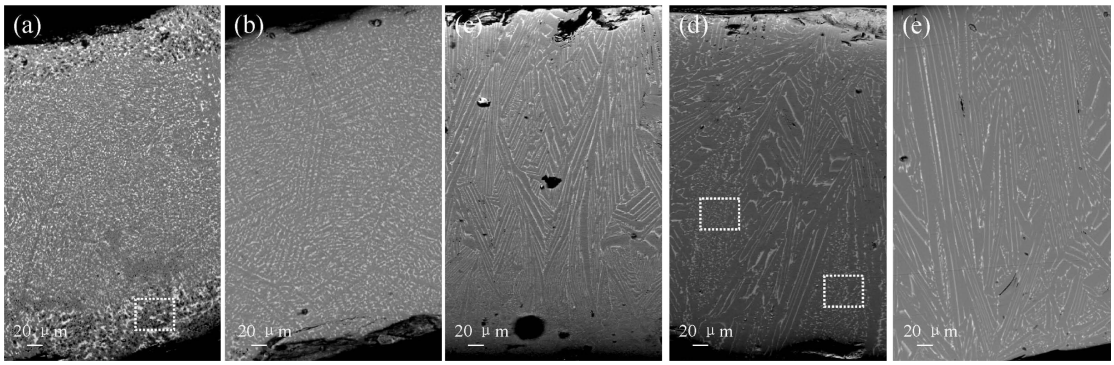

Fig. 1. The SEM images of the cross section for the strips of $Ce_{14}(Fe,M)_{79.7}Al_{0.5}B_{5.8}$ (a), $Ce_{14}(Fe,M)_{79.4}Al_{1.1}B_{5.5}$ (b), $Ce_{14}(Fe,M)_{78.9}Al_{1.6}B_{5.5}$ (c), $Ce_{14}(Fe,M)_{78.5}Al_{2.0}B_{5.5}$ (d) and Nd-Fe-B (e).

direction. Owing to the symmetry and anisotropy of crystal, the crystal generally grows fast along certain directions [25]. However, due to the poor crystal structure stability of $Ce_2Fe_{14}B$, the directional growth of crystals is interrupted by the competitive growth of heterophases.

As the content of Al increases to 1.6 at.%, the main phase of $Ce_2Fe_{14}B$ crystals is basically in strip shape (shown in Fig. 1(c)), which is originated from the crystal directional growth and the formation of columnar crystals [26]. $CeFe_2$ phase is basically linear distribution, thinly coating on the surface of the columnar crystal. The melting point of $Ce_2Fe_{14}B$ is high, while that of the intergranular phase $Ce(Fe,Al)_2$ is low and decreases with the increase of Al content [23]. $Ce_2Fe_{14}B$ crystals crystallize firstly in the rapid solidification, preferring to grow perpendicular to the crystal plane (410) along the cooling direction. The liquid phase of $CeFe_2$ is distributed on the surface of $Ce_2Fe_{14}B$ crystals, which may have well wettability and doesn't hinder the directional growth of $Ce_2Fe_{14}B$ crystals. As shown in Fig. 1(d), increasing the content of Al to 2.0 at.%, in some areas indicated in the box the $CeFe_2$ phases are distributed dispersedly without the formation of $Ce_2Fe_{14}B$ columnar crystals.

Fig. 1(e) is the SEM image of the cross section of Nd-(Fe,M)-B strip, and the microstructure of the columnar crystals is similar to that in Fig. 1(c). So in Ce-Fe-Al-B the columnar crystals could also be formed via adjusting the composition. Al is not only distributed in the intergranular phase, but also can enter into the main phase of $Ce_2Fe_{14}B$, and it may change the characteristics of both the main phase and the intergranular phase. The interference of the intergranular phase is weakened on the growth of $Ce_2Fe_{14}B$ crystals along preferred orientations, thus forming the columnar crystal structure.

In order to further probe the mechanism of columnar crystals formation, the heat absorption and phase transition temperature analysis were carried out via DSC for the Ce-Fe-Al-B strips. As shown in Fig. 2(a), there is a significant endothermic peak signified by the red arrow near 1100 °C, which corresponds to the melting point of $Ce_2Fe_{14}B$ crystals. With the increase of Al content, the melting point of the main phase increases slightly, indicating that the binding energy increases in the crystal and that the internal energy U decreases. As shown by the red arrow in Fig. 2(b), there is a weak endothermic peak near 150 °C, which corresponds to the Curie temperature of $Ce_2Fe_{14}B$ phase for the ferromagnetic to paramagnetic phase transition. There are no the visible endothermic peaks in $Ce_{14}(Fe,M)_{79.7}Al_{0.5}B_{5.8}$ and $Ce_{14}(Fe,M)_{79.4}Al_{1.1}B_{5.5}$ strips. The imperfection of ordered atomic arrangement and the crystal defects would affect the consistency of

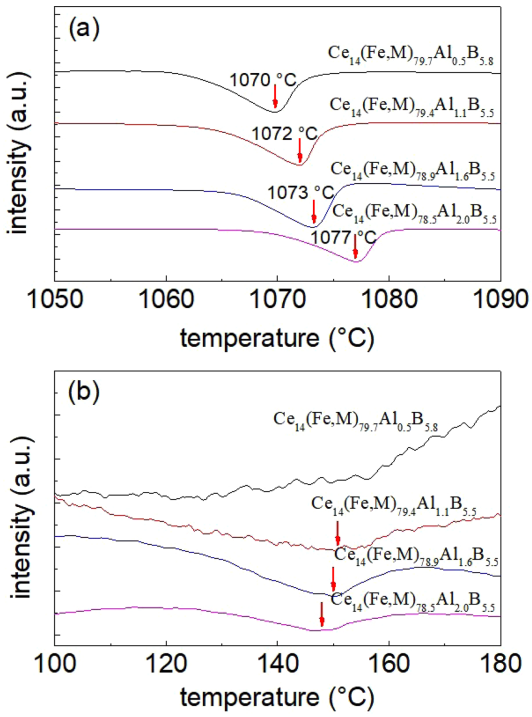

Fig. 2. (Color online) The heat absorption analysis at melting point (a) and Curie temperature (b) for the phase transition of Ce-Fe-Al-B strips.

electron exchange interaction and widen the phase transition temperature span [27, 28]. As the content of Al increases to 1.6 at.%, the endothermic peak is clear at Curie temperature in $Ce_{14}(Fe,M)_{78.9}Al_{1.6}B_{5.5}$, indicating that the crystal structure of ferromagnetic phase is relatively perfect due to the improvement of crystal structure stability, and so the ability of crystal directional growth is enhanced.

The XRD spectrums of powders are shown on Fig. 3 to further study the phase constitution. In addition to $Ce_2Fe_{14}B$ phase, there is also the impurity phase of $CeFe_2$ in these samples. The diffraction peak is wider at 2θ angle of 44.6° in $Ce_{14}(Fe,M)_{79.7}Al_{0.5}B_{5.8}$, which results from the overlap of diffraction peaks for α-Fe phase and $Ce_2Fe_{14}B$ phase. As the content of B is reduced and the content of Al is increased appropriately, the diffraction peak at 2θ angle of 44.6° becomes weak, verifying the elimination of α-Fe phase. The phase constitution on XRD analysis is consistent with the result observed in Fig. 1. It is noted that the diffraction peaks of $Ce_2Fe_{14}B$ phase are weaker in $Ce_{14}(Fe,M)_{79.7}Al_{0.5}B_{5.8}$, implying that the crystallinity is low and the crystal structure is imperfect [15], and so it is easy for the formation of impurity phases and the directional growth is difficult for $Ce_2Fe_{14}B$ crystal phase. For Al content of 1.1 at.%, the diffraction peaks of

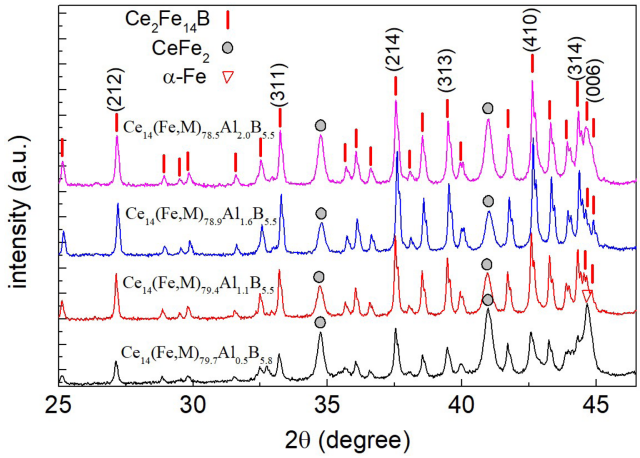

Fig. 3. (Color online) The powders XRD spectrums for the alloy strips.

$Ce_2Fe_{14}B$ phase is stronger, and as the content of Al increases to 1.6 at.% and 2.0 at.%, they become strongest, indicating that the structure stability of $Ce_2Fe_{14}B$ crystal is improved in $Ce_{14}(Fe,M)_{78.9}Al_{1.6}B_{5.5}$ and $Ce_{14}(Fe,M)_{78.5}Al_{2.0}B_{5.5}$. In $Ce_{14}(Fe,M)_{79.7}Al_{0.5}B_{5.8}$ the characteristic peaks of $CeFe_2$ are strong, which implies a large volume fraction of $CeFe_2$ phase in the strips. As the content of B is reduced and the content of Al is increased to 1.6 at.%, the characteristic peaks of $CeFe_2$ become weak, whereas the characteristic peaks become stronger for Al content of 2.0 at.% in $Ce_{14}(Fe,M)_{78.5}Al_{2.0}B_{5.5}$. The volume fractions of $Ce_2Fe_{14}B$, $CeFe_2$ and α-Fe phase are obtained by the Jade software and listed in Table 1. As the content of B is reduced and the content of Al is increased the corresponding angle of the diffraction peaks shift, indicating that the lattice constant and cell volume change, which results from the entrance of Al atoms into $Ce_2Fe_{14}B$ lattice [29]. The lattice constants are also listed in Table 1 according to the cell refinement by Jade software.

Al atoms enter into $Ce_2Fe_{14}B$ lattice, and due to the different atomic types the entropy *S* of the compound increases. The melting point increases and the internal energy *U* of the crystal decreases with the increase of Al content, so the free energy *F=U-TS* decreases, which is conducive to the structure stability and the directional growth of the crystals from the perspective of thermodynamics. Bearing this understanding in mind, the formation of α-Fe phase is suppressed, the crystallinity of $Ce_2Fe_{14}B$ phase is improved with the formation of columnar grains and the volume fraction of $Ce_2Fe_{14}B$ increases in $Ce_{14}(Fe,M)_{78.9}Al_{1.6}B_{5.5}$ strips. As the content of Al increases to 2.0 at.%, the volume fraction of $CeFe_2$ increases, and so some characteristics and the wettability change for $CeFe_2$ phase [23, 30, 31]. Due to the competitive growth between $CeFe_2$ and $Ce_2Fe_{14}B$ phases, the directional growth of $Ce_2Fe_{14}B$ crystals is hindered by the grain growth of $CeFe_2$ in $Ce_{14}(Fe,M)_{78.5}Al_{2.0}B_{5.5}$.

The microstructure of the strips would be inherited in the sintered magnets [32]. Through hydrogen decrepitation, jet milling, orientation pressing and sintering, the condensed sintered magnets were obtained for Ce-Fe-Al-B compounds. The XRD spectrums of powders are shown for the sintered magnets in Fig. 4. There are some differences between the XRD patterns of the sintered magnets and the strips, and there exist Ce-rich phase and Ce-oxide for the magnets. In the preparation of sintered magnets the atomic migration and diffusion are inevitable, especially in the sintering process. As shown in the Fig. 4, the diffraction peaks of $CeFe_2$ phase become weak, indicating that the amount of $CeFe_2$ phase is reduced. Fig. 5 shows the SEM images for the surface morphology in

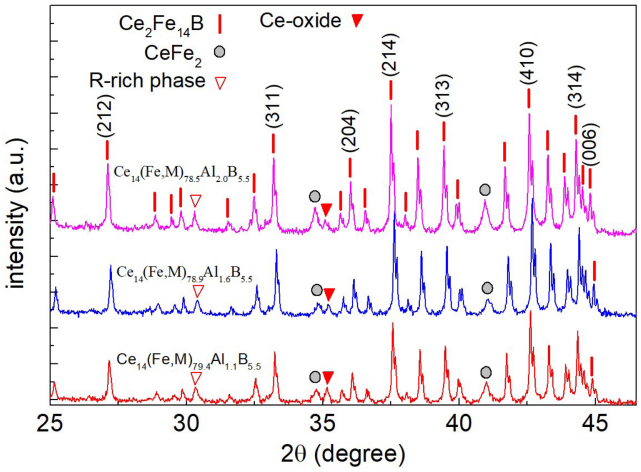

Fig. 4. (Color online) The powders XRD spectrums for the sintered magnets.

Table 1. The lattice constant and the volume fraction for the constitution phase in the strips.

Composition	Lattice constant a	Lattice constant c	Cell volume	$Ce_2Fe_{14}B$ fraction	$CeFe_2$ fraction	α-Fe_2 fraction
$Ce_{14}(Fe,M)_{79.7}Al_{0.5}B_{5.8}$	8.75 Å	12.11 Å	927.03 Å^3	63.5 vol.%	21.4 vol.%	15.1 vol.%
$Ce_{14}(Fe,M)_{79.4}Al_{1.1}B_{5.5}$	8.75 Å	12.12 Å	928.27 Å^3	87.3 vol.%	12.7 vol.%	
$Ce_{14}(Fe,M)_{78.9}Al_{1.6}B_{5.5}$	8.74 Å	12.11 Å	926.2 Å^3	92.5 vol.%	7.5 vol.%	
$Ce_{14}(Fe,M)_{78.5}Al_{2.0}B_{5.5}$	8.74 Å	12.13 Å	927.01 Å^3	83.9 vol.%	16.1 vol.%	

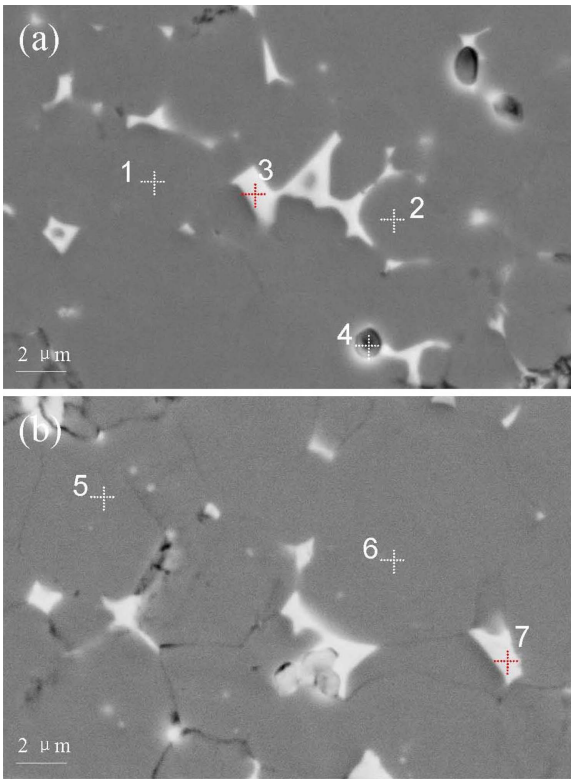

Fig. 5. (Color online) The SEM images of surface morphology for $Ce_{14}(Fe,M)_{79.4}Al_{1.1}B_{5.5}$ (a) and $Ce_{14}(Fe,M)_{78.9}Al_{1.6}B_{5.5}$ (b).

$Ce_{14}(Fe,M)_{79.4}Al_{1.1}B_{5.5}$ and $Ce_{14}(Fe,M)_{78.9}Al_{1.6}B_{5.5}$, and Table 2 lists the atomic percent contents of Nd, Fe, Al and oxygen for the marked points. Points 1, 2, 5 and 6 are inside the main phase, and the contents of Ce and Fe are close to those in $Ce_2Fe_{14}B$ phase. Points 3, 4 and 7 are in the intergranular phases, and the contents of Ce and Fe are close to those in $CeFe_2$ phase. Point 4 is in the Ce-oxide phase with high oxygen content. These facts on composition analysis are consistent with the phase constitution analysis on XRD patterns. It's important to note that the content of Al in the main phase is higher

Table 2. The atomic percent contents of Ce, Fe, Al and oxygen for spots in Fig. 5.

Contents / Spots	Ce (at.%)	Fe,M (at.%)	Al (at.%)	O (at.%)
1	13.18	85.3	0.6	0.32
2	13.3	85.13	0.62	0.33
3	29.17	69.27	0.31	0.94
4	49.3	25.16	0.28	24.98
5	12.52	84.22	1.72	1.54
6	12.7	84.01	1.73	1.56
7	27.52	67.22	0.93	4.33

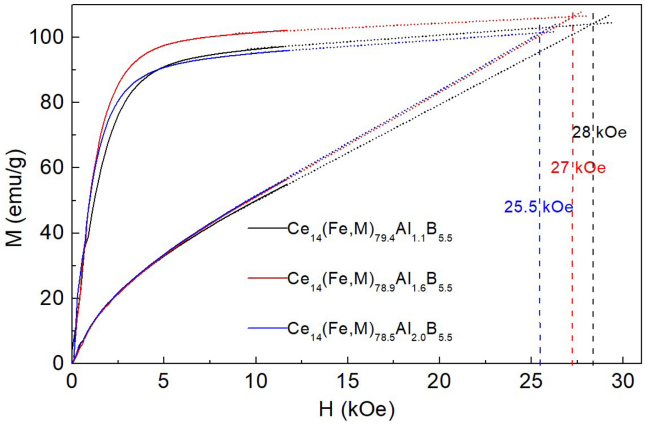

Fig. 6. (Color online) The magnetization curves along the easy magnetization axis and the hard magnetization axis and their extended line to the intersection point.

than that in the intergranular phase, implying that Al atoms prefer to enter into Ce-Fe-Al-B crystals for improving the crystal structure stability owing to the thermodynamics origin.

Fig. 6 shows the magnetization curves of the easy magnetization axis and the hard magnetization axis, respectively. The magnetization curves are extended to the intersection point, and the corresponding horizontal ordinate of the intersection point is the estimated value of the magnetocrystalline anisotropy field [33, 34]. In magnets of $Ce_{14}(Fe,M)_{79.4}Al_{1.1}B_{5.5}$ the estimate value is 28 kOe. With the increase of Al content, the anisotropy field just decreases slightly. In $Ce_{14}(Fe,M)_{78.9}Al_{1.6}B_{5.5}$ and $Ce_{14}(Fe,M)_{78.5}Al_{2.0}B_{5.5}$ they are 27 kOe and 25.5 kOe, respectively. According to the magnetization curve along the easy magnetization axis, the magnetization reaches to the saturation state at the applied magnetic field of about 10 kOe, and the fitting values of the saturation magnetization M_s are 104 emu/g, 106 emu/g and 101 emu/g, respectively, in magnets of $Ce_{14}(Fe,M)_{79.4}Al_{1.1}B_{5.5}$, $Ce_{14}(Fe,M)_{78.9}Al_{1.6}B_{5.5}$ and $Ce_{14}(Fe,M)_{78.5}Al_{2.0}B_{5.5}$. The saturation magnetization increases a slight in $Ce_{14}(Fe,M)_{78.9}Al_{1.6}B_{5.5}$, which is partially attributed to the increase in the volume fraction of ferromagnetic phase $Ce_2Fe_{14}B$ and the reduction in the volume fraction of $CeFe_2$ phase.

EBSD measurements were conducted on the orientation plane (001) to determine the crystal orientation [35, 36]. Fig. 7(a1) and (b1) show the diffraction quality diagram and phase distribution diagram for $Ce_{14}(Fe,M)_{79.4}Al_{1.1}B_{5.5}$ and $Ce_{14}(Fe,M)_{78.9}Al_{1.6}B_{5.5}$, respectively. The grains with green color are the $Ce_2Fe_{14}B$ crystal phase with perfect orientation in crystal plane (001), and those grains with gray color are poor in orientation. The areas with black

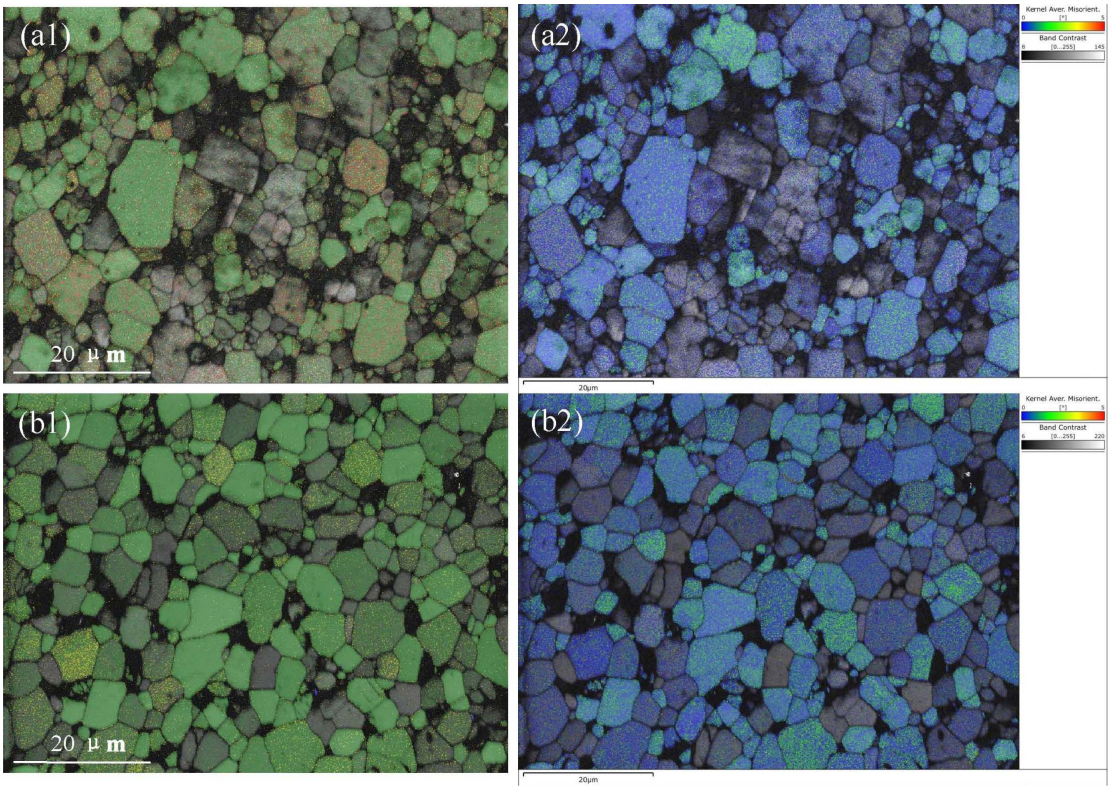

Fig. 7. (Color online) The diffraction quality diagram and phase distribution diagram for $Ce_{14}(Fe,M)_{79.4}Al_{1.1}B_{5.5}$ (a1) and $Ce_{14}(Fe,M)_{78.9}Al_{1.6}B_{5.5}$ (b1), and the local orientation difference for $Ce_{14}(Fe,M)_{79.4}Al_{1.1}B_{5.5}$ (a2) and $Ce_{14}(Fe,M)_{78.9}Al_{1.6}B_{5.5}$ (b2).

color imply other substances, such as Ce-rich phase, Ce-oxide and $CeFe_2$ phase that the instrument can't identify [37]. The grain boundary is also very clear due to the grain boundary phase and grain boundary defects. In Fig. 7(a1), the amount of gray and black areas is larger, indicating that the volume fraction of impurity phases is larger and that the orientation is relatively not perfect along the easy magnetization direction. Fig. 7(a2) and (b2) show the local orientation difference in $Ce_{14}(Fe,M)_{79.4}Al_{1.1}B_{5.5}$ and $Ce_{14}(Fe,M)_{78.9}Al_{1.6}B_{5.5}$ magnets. For blue grains the deviation of the orientation angle along axis [001] is small, while for gray grains that is large. The amount of gray grains is less on Fig. 7(b2), indicating a better orientation in $Ce_{14}(Fe,M)_{78.9}Al_{1.6}B_{5.5}$ magnets. The good orientation degree is related to the directional growth of $Ce_2Fe_{14}B$ crystals and the formation of columnar crystals in $Ce_{14}(Fe,M)_{78.9}Al_{1.6}B_{5.5}$ strips [16]. In addition, the microstructure is more homogeneous and grain sizes are less than 7 μm in $Ce_{14}(Fe,M)_{78.9}Al_{1.6}B_{5.5}$ strips, whereas in $Ce_{14}(Fe,M)_{79.4}Al_{1.1}B_{5.5}$ the sizes of some grains are much larger. Appropriate amount of Al addition would lead to the regular and periodic microstructure with the formation of columnar grains in the strips, which is beneficial to the formation of the more homogeneous microstructure in sintered magnets.

4. Conclusions

In summary, via reducing properly the content of B in the Ce-Fe-Al-B compound and increasing the content of Al, the impurity phase of α-Fe is eliminated in the strips prepared by rapid solidification. The main phase of $Ce_2Fe_{14}B$ crystals can grow along preferred direction to form columnar crystals in the $Ce_{14}(Fe,M)_{78.9}Al_{1.6}B_{5.5}$ compound. The formation of columnar crystals results from the symmetry and anisotropy of crystals, and the directional growth could be interrupted by the competitive growth of multiple grains and the growth of heterogeneous phases. The content of Al in the $Ce_2Fe_{14}B$ lattice is higher than that in the intergranular phase owing to the thermodynamic properties. With the increase of Al content, the melting point of $Ce_2Fe_{14}B$ crystal increases, indicating that the binding energy of the crystal increases and the internal energy U decreases. The entropy S increases in the Ce-Fe-Al-B compound, and the free energy F reduces, which is conducive to the stability of the crystal structure and the crystal directional growth. The formation of columnar crystals is beneficial to the

preparation of single crystal particles and the orientation of the easy magnetization axes in sintered magnets. These investigations pave a way to solve the difficulty in the directional growth of $Ce_2Fe_{14}B$ crystals and establish the experimental basis for the preparation of rare-earth Ce-based magnets.

Acknowledgements

The present work was supported by the State Key R&D Program of China (Grant No. 2021YFB3500100), the National Natural Science Foundation of China (Grant Nos. 52461035, U23A20550, 12464014), the Inner Mongolia Autonomous Region Natural Science Foundation (Grant No. 2024MS05045), the Fundamental Research Funds for Inner Mongolia University of Science & Technology (Grant No. 2023RCTD005), and the Scientific Research Special Project for First-Class Disciplines in Inner Mongolia Autonomous Region (YLXKZX-NKD-001).

References

[1] J. F. Herbest, Rev. Mod. Phys. **63**, 819 (1991).
[2] M. Sagawa, S. Fujimura, H. Yamaoto, and Y. Matsuura, IEEE Trans. Magn. **20**, 1584 (1984).
[3] O. Gutfleisch, M. A. Willard, B. Ekkes, C. H. Chen, S. G. Sankar, and J. P. Liu, Adv. Mater. **23**, 821 (2011).
[4] J. F. Herbest, M. S. Meyer, and F. E. Pinkerton, J. Alloys Compd. **111**, 07A718 (2012).
[5] A. K. Pathak, M. Khan, K. A. Gschneidner Jr., R. W. McCallum, L. Zhou, K. Sun, M. J. Kramer, and V. K. Pecharsky, Acta. Mater. **103**, 211 (2016).
[6] D. W. Duan, L. Wei, Z. B. Li, Q. Zhao, and Y. F. Li, J. Magn. **26**, 194 (2021).
[7] Y. Li, J. Q. Yan, B. C. Sales, and D. S. Parker, Phys. Rev. Appl. **17**, 064020 (2022).
[8] J. F. Xiong, D. Liu, X. Q. Zheng, L. C. Wang, X. Ming, J. Z. Hao, H. Bai, Y. Yin, J. F. Xi, B. H. Li, T. Y. Zhao, F. X. Hu, J. R. Sun, J. Shen, and B. G. Shen, J. Alloys Compd. **985**, 174095 (2024).
[9] D. Goll, M. Boettle, J. Buschbeck, R. Loeffler, and G. Schneider, Phys. Status Solidi RRL. **18**, 2400151 (2024).
[10] E. Niu, Z. Chen, Y. G. Zhao, J. Zhang, X. L. Rao, B. P. Hu, and Z. X. Wang, J. Appl. Phys. **115**, 113912 (2014).
[11] X. H. Shao, X. Q. Zhou, S. H. Liang, C. Yang, Y. S. Que, B. Guo, H. P. Bao, G. C. Tang, X. L. Yan, J. S. Bao, L. S. Qin, K. Y Shu, D. Chen, and D. L. Peng, J. Alloys Compd. **1014**, 178567 (2025).
[12] C. J. Yan, S. Guo, R. J. Chen, D. Lee, and A. R. Yan, Chin. Phys. B. **23**, 107501 (2014).
[13] K. Orimoloye, D. Kevorkov, and M. Medraj, J. Alloys Compd. **763**, 289 (2018).
[14] A. H. Li, W. Yang, H. B. Feng, X. S. Chen, M. G. Zhu, and W. Li, IEEE Trans. Magn. **56**, 2101005 (2020).
[15] Z. B. Li, D. S. Wang, Z. X. Zhang, X. F. Zhang, F. X. Hu, J. R. Sun, and B. G. Shen, J. Alloys Compd. **729**, 988 (2017).
[16] J. Bernardi, J. Fidler, M. Sagawa, and Y. Hirose, J. Appl. Phys. **83**, 6396 (1998).
[17] J. Han, and Y. S. Wang, Materials Science and Technology, **7**, 213 (1999).
[18] K. Khlopkov, O. Gutfleisch, D. Eckert, D. Hinz, B. Wall, W. Rodewald, K. H. Müller, and L. Schultz, J. Alloys Compd. **365**, 259 (2004).
[19] C. J. Yan, S. Guo, R. J. Chen, D. Lee, and A. R. Yan, IEEE Trans. Magn. **50**, 2104604 (2014).
[20] D. Y. Wang, A. H. Li, H. B. Feng, and W. Li, Heliyon. **10**, e27245 (2024).
[21] M. Sagawa, J. Mater. Eng. Perform. **22**, 2860 (2013).
[22] D. Liu, T. Y. Zhao, J. Y. Jin, T. Y. Ma, J. F. Xiong, B. G. Shen, F. X. Hu, and J. R. Sun, Sci. China-Phys. Mech. Astron. **65**, 247511 (2022).
[23] L. L. Xi, A. H. Li, H. B. Feng, M. Tan, M. G. Zhu, and W. Li, J. Alloys Compd. **782**, 723 (2019).
[24] D. Goll, R. Loeffler, M. Boettle, J. Buschbeck, and G. Schneider, Materials. **17**, 3110 (2024).
[25] Y. Tao, and C. L. Degen, Nat. Commun. **9**, 339 (2018).
[26] N. T. Oster, D. T. Cavanaugh, K. W. Dennis, M. J. Kramer, R. W. McCallum, and I. E. Anderson, J. Appl. Phys. **111**, 07A723 (2012).
[27] I. S. Golovina, M. Falmbigl, C. J. Hawley, A. J. Ruffino, A. V. Plokhikh, I. A. Karateev, T. C. Parker, A. G. Perez, A. L. Vasilievd, and J. E. Spanier, Nanoscale. **10**, 21798 (2018).
[28] Z. B. Li, L. L. Zhang, X. F. Zhang, Y. F. Li, Q. Zhao, T. Y. Zhao, and B. G. Shen, J. Phys. D: Appl. Phys. **50**, 015002 (2017).
[29] K. Orimoloye, D. H. Ryan, F. E. Pinkerton, and M. Medraj, Appl. Sci. **8**, 205 (2018).
[30] J. Y. Jin, Z. H. Zhang, L. Z. Zhao, B. X. Peng, Y. S. Liu, J. M. Greneche, and M. Yan, Scr. Mater. **170**, 150 (2019).
[31] D. F. Franceschini and S. F. Da cunha, J. Magn. Magn. Mater. **51**, 280 (1985).
[32] Y. J. Zhang, T. Y. Ma, J. Y. Jin, J. T. Li, C. Wu, B. G. Shen, and M. Yan, Acta. Mater. **128**, 22 (2017).
[33] B. C. Li, J. Z Zhao, C. Wang, Y. L. Liu, S. Bai, and Z. B. Li, J. Magn. **30**, 12 (2025).
[34] M. Yue, W. Q. Liu, D. T. Zhang, Z. G. Jian, A. L. Cao, and J. X. Zhang, Appl. Phys. Lett. **94**, 092501 (2009).
[35] T. G. Woodcock, K. Khlopkov, A. Walther, N. M. Dempsey, D. Givord, L. Schultz, and O. Gutfleisch, Scr. Mater. **60**, 826 (2009).
[36] L. L. Zhang, M. G. Zhu, Y. J. Guo, L. W. Song, and W. Li, J. Alloys Compd. **891**, 161921(2021).
[37] T. G. Woodcock and O. Gutfleisch, Acta. Mater. **59**, 1026 (2011).